Available online at www.sciencedirect.com
ScienceDirect
Electrochimica Acta 53 (2008) 6978–6987
ELECTROCHIMICA Acta
www.elsevier.com/locate/electacta

Ternary $Cd_xZn_{1-x}Se$ deposited on Ag (1 1 1) by ECALE: Electrochemical and EXAFS characterization

F. Loglio [a,1], A.M. Telford [a], E. Salvietti [a], M. Innocenti [a,1], G. Pezzatini [a], S. Cammelli [b], F. D'Acapito [b], R. Felici [c], A. Pozzi [a], M.L. Foresti [a,*,1]

[a] *Dipartimento di Chimica, Università di Firenze, Via della Lastruccia 3, 50019 Sesto Fiorentino (FI), Italy*
[b] *CNR-INFM-OGG c/o ESRF, GILDA CRG, 6 Rue Jules Horowitz, F-38043, Grenoble, France*
[c] *Beamline Responsible, ID03 ESRF 6 rue J. Horowitz BP 220F-38043 Grenoble Cedex 9, France*

Received 31 October 2007; received in revised form 11 January 2008; accepted 13 January 2008
Available online 31 January 2008

Abstract

This paper reports the characterization of ternary II–VI semiconductor nanocrystals, deposited by the electrochemical atomic layer epitaxy (ECALE) technique.

In particular, morphological and structural properties of the ternary compounds of formula $Cd_xZn_{1-x}Se$ deposited on Ag (1 1 1) have been characterized as a function of composition. The number of the attainable x values is limited by the necessity of using well-defined ZnSe/CdSe deposition sequences. However, the quantitative analysis carried out on the basis of both electrochemical and extended X-ray absorption fine structure (EXAFS) experiments indicates that the ECALE method is a successful way of controlling the composition of $Cd_xZn_{1-x}Se$. In addition, the electrochemical measurements show that the amount of deposition is minimum in correspondence to the compound with $x = 0.5$, thus corroborating the hypothesis of a higher degree of disorder suggested both by morphological and structural investigation. The morphology was studied by atomic force microscopy (AFM). The structure of the films is estimated by EXAFS which is a powerful technique for the analysis of the local structure around chosen atoms.

Keywords: ECALE; AFM; Ternary $Cd_xZn_{1-x}Se$; Silver single crystals; EXAFS

1. Introduction

One of the goals of the present-day research is to decrease the size of the various components which make up electronic devices. This miniaturization is desirable not only in the electronic and optoelectronic industries, but more generally for the realization of new functional and smart materials. Such materials depend, to a large extent, on the possibility of controlling the formation of the material at the nanoscopic scale. Today electrochemistry extends to the domain of material science by developing electrochemical methods for material electrodeposition with control down to an atomic level. The advantages are mainly connected with good selectivity, low costs and low levels of wastestreams. The drawbacks are the necessity of conductive substrates and the use of condensed media that increases the presence of impurities [1].

Electrodeposition allows for the very precise control of material deposited through, for example, Faraday's law or through the use of self-limiting phenomena such as those involved in the underpotential deposition (UPD). Underpotential deposition is the basis of the electrochemical atomic layer epitaxy (ECALE) method proposed by Stickney and Gregory [2] for the deposition of well-ordered II–VI compounds. In the ECALE procedure, the binary compounds are obtained by alternating the underpotential depositions of the metallic and non-metallic elements. One major advantage of ECALE method consists in the possibility of separately optimizing the different steps of the alternate electrodeposition by adjusting the experimental parameters.

The deposition of ternary II–VI compounds offers the possibility of tuning the bandgap to meet specific needs, but poses the challenge of controlling the film composition. As reported

* Corresponding author. Tel.: +39 055 457 3107; fax: +39 055 457 3385.
E-mail address: foresti@unifi.it (M.L. Foresti).
[1] ISE member.

0013-4686/$ – see front matter © 2008 Elsevier Ltd. All rights reserved.
doi:10.1016/j.electacta.2008.01.046

by Wang's review on the nanostructures of II–VI compound semiconductors [3], cadmium selenides quantum dots demonstrate a strong size dependence on their physical properties. In particular, it has been shown that it is possible to correlate the quantum confinement of small crystallites of CdSe to an induced higher energy shift with decreasing size [4–7]. To improve quantum efficiency, the CdSe nanocrystal core is often passivated by another semiconductor shell with a higher energy band gap, such as ZnSe [8].

Thin films of ternary compounds like $Cd_xZn_{1-x}Se$ have been grown by different techniques. In particular, Han and Knoll prepared a solid solution of nanocrystals by heat treatment [9] and the mechanism for solid solution formation was elucidated by the recent work of Sung et al. [10].

In our laboratory, experience in the ECALE growth of ternary II–VI compound semiconductors was obtained by depositing $Cd_xZn_{1-x}S$ and $CdS_xSe_{(1-x)}$ on Ag (1 1 1) [11–13]. Both compounds were obtained by a procedure corresponding to the alternate deposition of the corresponding binary compounds in submonolayer amounts. Thus, the compound stoichiometry depends on the ZnS/CdS or on the CdS/CdSe deposition sequence in a well-defined and reproducible way, with the limit that only certain discrete x values are attainable. However, the quantitative analysis carried out by XPS and electrochemical stripping experiments indicates that the ECALE method has good control over composition. Then, photoelectrochemical measurements confirmed that the bandgap values of the obtained compounds vary about linearly with the composition parameter x which agrees with literature data reported for bulk materials.

This paper reports a detailed analysis on the growth of $Cd_xZn_{1-x}Se$ by alternating the ECALE deposition of the corresponding binary compounds. The experimental conditions for the deposition of both ZnSe and CdSe on Ag (1 1 1) by ECALE, as well as some preliminary results on the attainment of $Cd_xZn_{1-x}Se$ had been reported before [14,15,11].

The characterization includes the electrochemical characterization, the evaluation of composition by differential pulse anodic stripping analysis (DPASV) on hanging mercury drop electrode, the morphological analysis by atomic force microscopy (AFM) and the structural investigation by extended X-ray absorption fine structure (EXAFS) [16].

2. Experimental

2.1. ECALE film deposition

Fluka analytical reagent grade $Na_2SeO_3{\cdot}5H_2O$, Merck analytical reagent grade $3CdSO_4{\cdot}8H_2O$, $ZnSO_4{\cdot}7H_2O$, $HClO_4$, NH_4OH, $CH_3COONa{\cdot}3H_2O$ and CH_3COOH were used without further purification. Merk Suprapur NaOH and $HClO_4$ and NH_4OH were used to prepare the pH 8.5 ammonia buffer, whereas $CH_3COONa{\cdot}3H_2O$ and CH_3COOH were used to prepare the pH 5.5 acetic buffer. Merck $Na_4P_2O_7{\cdot}10H_20$ was recrystallized twice from bidistilled water and then dried. The solutions were freshly prepared just before the beginning of each series of measurements. An automated deposition apparatus consisting of Pyrex solutions reservoirs, solenoid valves, a distribution valve and a flow-cell was used under the control of a computer. The electrolytic cell was a Teflon cylinder with a 6.7 mm inner diameter and a 37 mm outer diameter, whose inner volume, about 0.8 ml, was delimited by the working electrode on one side and the counter electrode on the other side. The inlet and the outlet for the solutions were placed on the side walls of the cylinder. The counter electrode was gold foil, and the reference electrode was an Ag/AgCl (sat. KCl) placed on the outlet tubing. Both the distribution valve and the cell were designed and realized in the workshop of our Department [17]. The solution is pushed into the cell by applying a pressure as low as 0.3 atm which determines a flow-rate of about 1 ml s^{-1}. When the cell is filled, the pressure is no more applied, so that the flow is stopped during ECALE depositions. A simple homemade software allows filling the cell with the different solutions with the sequence necessary to obtain the compound. Binary compounds are simply obtained by alternating the underpotential deposition of the metallic element with the underpotential deposition of the non-metallic element in a cycle. Ternary compounds, such as cadmium and zinc chalcogenides, require of further alternating the cation deposition, which corresponds to alternate the deposition of the corresponding binary compounds. In other word, as better described later, cadmium and zinc selenide is obtained by alternating the deposition of CdSe and ZnSe. The silver single crystals were prepared according to the Bridgeman technique and polished by a CrO_3-based procedure preparation [18–21].

2.2. EXAFS measurements

EXAFS measurements at the Se–K (12658 eV) and Zn–K (9659 eV) edges were carried out at the GILDA-CRG beamline [22] of the European Synchrotron Radiation Facility in Grenoble. The photon energy selection was carried by a fixed exit monochromator equipped with a pair of Si (3 1 1) crystals running in dynamical focusing mode [23]. Two Pd-coated mirrors, set to an energy cutoff of 21 keV, were used for the harmonics rejection. The intensity of the beam impinging on the sample was monitored with an Ar filled ion chamber. The fluorescence spectra was measured using a single element Hyperpure Ge detector and the Se-Kα and Zn-Kα emission lines were selected for the collection of the EXAFS spectra at the related edges. 2 spectra per sample were collected and averaged in order to limit instrumental uncertainties to the data.

2.3. AFM measurements

Topography was measured ex situ in a dry nitrogen atmosphere, using a Molecular Imaging AFM (PicoSPM, Molecular Imaging) operating in contact mode, with a commercial Si_3N_4 cantilever (Nanosensors, Wetzlar-Blankenfeld). The samples were characterized by non-filtered 512 × 512 pixels images of 5 μm × 5 μm.

3. Results and discussion

3.1. Se deposition on Ag (1 1 1) and on Ag (1 1 1) covered by a UPD layer of either Cd or Zn

Due to the instability of selenide solutions, Se_{UPD} layers cannot be directly obtained through oxidative underpotential deposition. On the contrary, the suggested procedure to obtain an UPD layer of selenium consists of depositing an excess of Se(0) from 0.5 mM Na_2SeO_3 solutions and then applying a potential, of about −0.9 V, which is sufficient to reduce bulk selenium, but not the UPD layer [14]. In spite of the two-step procedure, the experimental conditions for the attainment of Se_{UPD} on Ag (1 1 1) are not critical. In fact, the optimum potential for Se deposition from pH 8.5 ammonia buffer solutions ranged from −0.86 to −0.9 V [15].

The electrochemistry of Se(IV) on Ag (1 1 1) has been thoroughly investigated in our laboratory [24] and the voltammetric curves obtained on the single crystal were interpreted with the help of the corresponding mass variations as obtained by nanobalance measurements on polycrystalline silver. In agreement with some observations already reported in the literature [25–28], our analysis confirmed the presence of two different Se(IV) electroreduction pathways: the first one involving four electrons and leading to Se(0), and the second one involving six electrons and leading to Se(−II). However the direct electroreduction yields "gray" electroinactive Se(0), whereas the only electroactive form of Se(0) seems to be the "red" selenium which is obtained by the chemical comproportionation reaction between Se(IV) and Se(−II). At first, Se(−II) is that formed by the six electrons reduction scheme, but in a short time the amount of Se(−II) dramatically increases, since it also originates by the concomitant "red" Se(0) reduction. Our analysis suggested the existence of two competitive processes: the first one leading to the formation of "red" Se(0), and the second one leading to its reduction. Curve a in Fig. 1 shows the attainment of stationary conditions in the process of Red Se(0) formation and its successive reduction to Se(−II) on Ag (1 1 1) [24].

A short analysis of Se(IV) electrochemical behavior on Ag (1 1 1) covered by a UPD layer of either Cd or Zn, showed that the same two-step procedure can be applied for obtaining the UPD layer of Se. Therefore, all UPD layers of Se were obtained by depositing bulk Se(0) at $E = -0.87$ V and then destroying the amount of Se(0) exceeding the UPD layer at $E = -0.9$ V. This did not depend on which underlying substrate was used.

3.2. Procedure of ECALE deposition of $Cd_xZn_{1-x}Se$

As reported before, the experimental procedure to obtain $Cd_xZn_{1-x}Se$ with different x values consists of alternating ZnSe and CdSe ECALE cycles with different deposition sequences [11]. To obtain CdSe, Cd was deposited at underpotential on the previously deposited Se. Curve b in Fig. 1 shows the reductive underpotential deposition of Cd on a Se-covered Ag (1 1 1) substrate from a 1 mM Cd(II), 0.01 M pyrophosfate and 0.01 M NaOH pH 12 solution. As suggested from the figure, the Cd_{UPD} layer was obtained by applying a potential $E = -0.7$ V for 60 s. After Cd deposition, the cell was rinsed with ammonia buffer. In an analogous way, ZnSe was obtained by depositing Zn at $E = -0.8$ V, as suggested by the reductive underpotential deposition of Zn from 1 mM Zn(II) solutions in acetic buffer (curve c in Fig. 1).

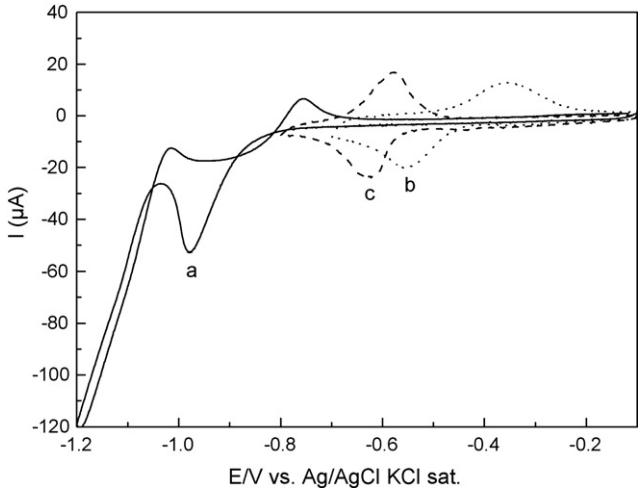

Fig. 1. (curve a) Cyclic voltammogram of 8×10^{-4} M Se(IV) solutions in pH 8.5 ammonia buffer recorded from −0.1 to −1.2 V vs. Ag/AgCl sat. on Ag (1 1 1) after the attainment of stationary conditions; (curve b) reductive underpotential deposition of Cd on a Se-covered Ag (1 1 1) substrate from a 1 mM Cd(II), 0.01 M pyrophosfate and 0.01 M NaOH pH 12 solution; (curve c) reductive underpotential deposition of Zn on a Se-covered Ag (1 1 1) substrate from 1 mM Zn(II) solutions in acetic buffer. The scan rate is 50 mV s^{-1}.

However, the compound obtained by alternating one CdSe ECALE cycle with one ZnSe ECALE cycle yields a compound with a very high percentage of Cd (74%) in place of the 50% expected value, even though XPS analysis revealed the expected 1:1 stoichiometric ratio between cations (i.e. Cd + Zn) and Se. Then, as already observed [11,13], the most effective way to increase the amount of Zn in the deposit consists of depositing more ZnSe cycles per CdSe cycle. Therefore the basic ECALE cycles are combined as to give different ZnSe/CdSe deposition sequences, and each deposition sequence can be repeated as many times as desired to obtain deposits of practical importance.

In this paper, a systematic investigation was carried out with ZnSe/CdSe deposition sequences ranging from 1 to 8:

$$\text{ZnSe/CdSe} = 1: \text{Se/Cd/Se/Zn/Se/Cd/Se/Zn/Se/Cd/Se/Zn/Se/Cd/Se/Zn/}\ldots$$

$$\text{ZnSe/CdSe} = 2: \text{Se/Cd/Se/Zn/Se/Zn/Se/Cd/Se/Zn/Se/Zn/Se/Cd/Se/Zn/}\ldots$$

$$\text{ZnSe/CdSe} = 5: \text{Se/Cd/Se/Zn/Se/Zn/Se/Zn/Se/Zn/Se/Zn/Se/Cd/Se/Zn/}\ldots$$

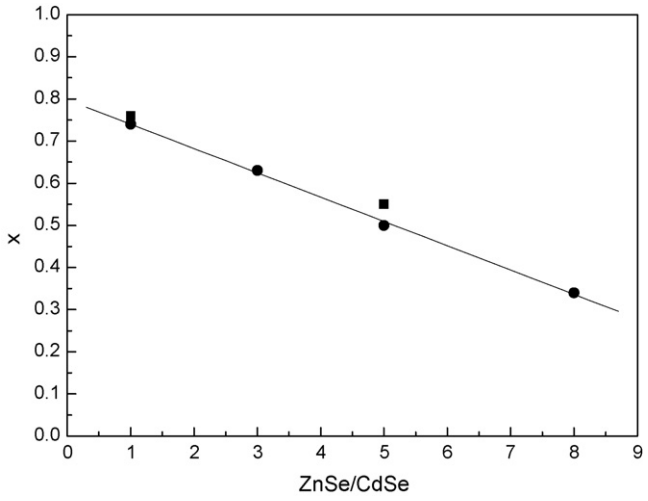

Fig. 2. Plot of the x stoichiometric parameter as a function of the ZnSe/CdSe deposition sequence as obtained by DPASV (●) and EXAFS measurements (■).

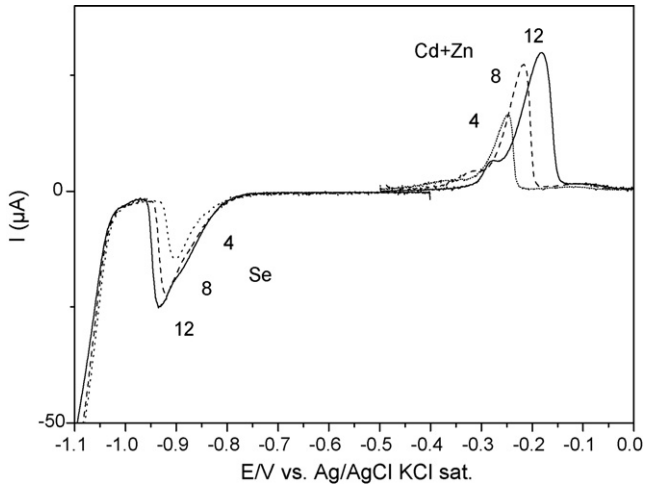

Fig. 3. Linear sweep voltammograms for the oxidative strippings of 4, 8 and 12 (Zn + Cd) layers and the reductive strippings of the corresponding Se layers, for the ZnSe/CdSe deposition sequence equal to 3. The scan rate is 10 mV s^{-1}.

$$\text{ZnSe/CdSe} = 8: \text{Se/Cd/Se/Zn/Se/Zn/Se/Zn/Se/Zn}$$
$$\text{/Se/Zn/Se/Zn/Se/Zn/Se/Zn/}\ldots\text{/Se/Cd}\ldots$$

3.3. Stoichiometry of the ternary sulfides obtained with different deposition sequences

The stoichiometry of the compounds obtained with the ZnSe/CdSe sequence equal to 1, 3, 5 and 8 was determined by classical quantitative analysis: the deposits were dissolved in 5 ml of 0.1 M HCl, where selenium is eliminated as H_2Se. Then the amount of cation was determined by DPASV on hanging mercury drop electrode. Fig. 2 shows that the x stoichiometric parameter is a linear function of the ZnSe/CdSe sequence. The linear behavior is confirmed by the x values derived from EXAFS measurements for the ZnSe/CdSe sequence equal to 1 and 5. All samples were obtained with approximately 100 ECALE cycles, whatever the deposition sequence used. The composition measurements well fit the stoichiometries determined before for the ZnSe/CdSe sequences equal to 1, 3 and 8 by ex situ X-ray photoelectron spectroscopy (XPS) in ultra-high vacuum [11]. As already reported [11–13], the stoichiometry of the ternary compounds depends on the deposition sequence and this is evidenced to be a well-defined and reproducible trend. The linear behavior of the plot allows for a good estimation of the x values not directly measured.

3.4. Electrochemical characterization

As usual, the first characterization of the ternary compound obtained is the electrochemical characterization [17]. This is carried out, in situ, by scanning the potential to values where the deposits are destroyed. As for the binary compounds, the charge obtained by integrating the stripping peaks obtained with different numbers of basic ECALE cycles (either of CdS or ZnS) gives the amount of the elements deposited for that number of cycles. As an example, Fig. 3 reports the stripping curves of deposits obtained with a ZnSe/CdSe sequence equal to 3, and with increasing number of ECALE cycles. Numbers on each curve indicates the number of deposition cycles. Of course in the case of the cations, the numbers indicate the sum of Cd and Zn. This procedure was applied to the deposits obtained with ZnSe/CdSe deposition sequences equal to 1, 2, 3, 5, 7 and 8.

The charge involved in the stripping increases linearly with the number of deposition cycles. However, regardless of the stoichiometry of the ternary compound obtained, the charge involved in stripping the cations equals the charge involved in stripping the anion, thus indicating the right 1:1 stoichiometric ratio. As an example, Fig. 4 shows that this occurs even in the case of the extreme deposition sequence ZnSe/CdSe = 8. Note that in this case the plot is limited to 3 points since the cation/anion balance can be done only every 9 ECALE cycles. Yet, the slope of the plot changes while changing the ZnSe/CdSe sequence. More particularly, plotting these slopes against the stoichiometric x parameter, a minimum at $x = 0.5$ is observed,

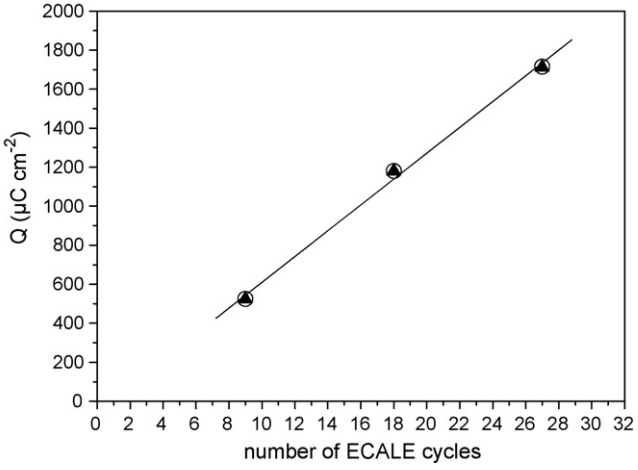

Fig. 4. Plots of the charges involved in the oxidative stripping of (Zn + Cd) (▲) and Se (◯) as a function of the number of ECALE cycles for the ZnSe/CdSe deposition sequence equal to 8.

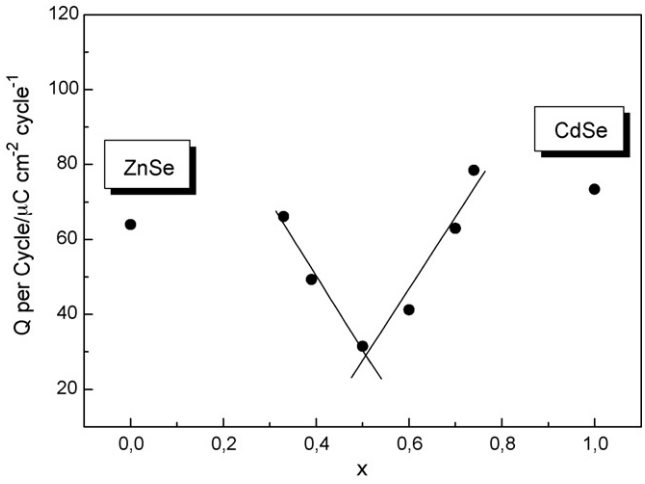

Fig. 5. Plot of the charge per cycle as obtained by either the oxidative stripping of (Zn + Cd) or the reductive stripping of Se as a function of the stoichiometric parameter x.

with two symmetrical branches around the minimum (Fig. 5). The figure also shows the values obtained for the binary Zn and Cd selenides [14,15]. This behavior is not monotonic and therefore it cannot be ascribed to the increasing (or decreasing) percentage of just one of the two cations.

Now, it must be stressed that each slope plotted in Fig. 5 gives the total amount of cations (or of Se) deposited in each deposition cycle for that deposition sequence. As a consequence, it is evident the presence of a limiting factor that occurs in the x range between 0.3 and 0.7 and is maximum for $x = 0.5$. These stoichiometric values coincide with those reported in the literatures [29,30] for the ranges of existence of the different structures ascribed to the $Cd_xZn_{(1-x)}Se$ thin films:

$$\begin{aligned} &\text{Zincblend (cubic)} \quad \text{for } 0 \le x < 0.3, \\ &\text{Cubic + hexagonal} \quad \text{for } 0.3 < x \le 0.8, \\ &\text{Wurtzite (hexagonal)} \quad \text{for } 0.8 < x \le 1 \end{aligned}$$

In other words, we can assume that when the percentage of Zn in the compound is approximately equal to that of Cd, the different structures are present in a comparable amount, thus suggesting a structural disorder that could be responsible for a reduced amount of deposition. In the following it will be shown that such disorder is also indicated by the EXAFS measurements. The EXAFS data also indicate strong differences in the Zn–Se and Cd–Se bond length values.

3.5. Assessment of the experimental conditions for deposition and current profiles

Good experimental conditions for deposition require that the charges involved in the UPD layers of each element do not undergo appreciable changes during the whole process of deposition. In our experiments, the turbulence in correspondence of the solution exchanges, operated by means of a suitable pressure, prevents the accurate measurement of the charge during deposition. Therefore, as already shown, we usually measure the stripping charges flowing when the deposits are destroyed.

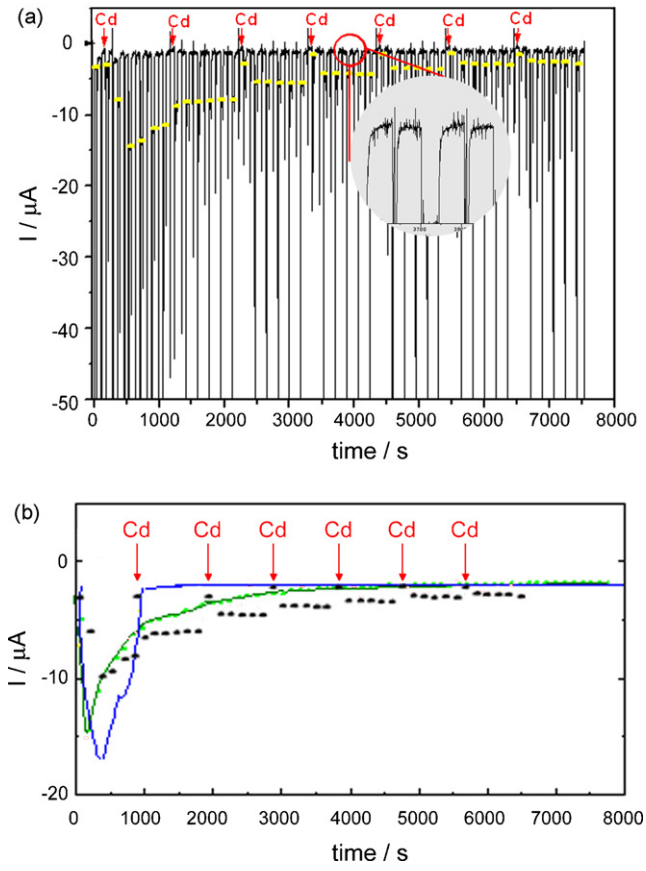

Fig. 6. (a) Reports the current flowing during deposition as a function of time for the ZnSe/CdSe sequence equal to 5. Spikes in the cathodic currents indicate the solutions changes and the highlighted profile is that of the bulk Se deposition. The sharp decrease every 5 cycles identifies bulk Se deposition on Cd. (b) Current profiles of bulk Se deposition as in Fig. 6a (a, red dots), CdSe (curve b, blue line), and ZnSe (curve c, green line). (For interpretation of the references to color in this figure legend, the reader is referred to the web version of the article.)

To limit the possibility that the experimental conditions could appreciably vary during deposition, becoming critical, the potentials chosen for deposition should ensure UPD conditions also going on with the number of ECALE cycles. More precisely, in our opinion, the potentials should be as close as possibly to bulk deposition, still remaining in the UPD region. For example, referring to Fig. 1, note that the potential chosen for Zn deposition, −0.8 V, is much more negative than the potential, −0.62 V, of the UPD peak, and the potential chosen for Cd deposition, −0.7 V, is again much more negative than the potential, −0.52 V, of the UPD peak. Analogous criteria were applied for the deposition of bulk Se(0) excess and its successive reduction necessary to obtain the UPD layer. Then, the evidence that the conditions did not vary while increasing the number of ECALE cycles is given by the linear increase of the charge with the number of deposition cycles, which indicates that the same amount of compound is deposited in each deposition cycle.

A large part of the literature on ECALE stresses the necessity of reaching “steady-state conditions”, thus indicating the attainment of a reproducible current profile during deposition. Therefore, even though we choose the experimental conditions

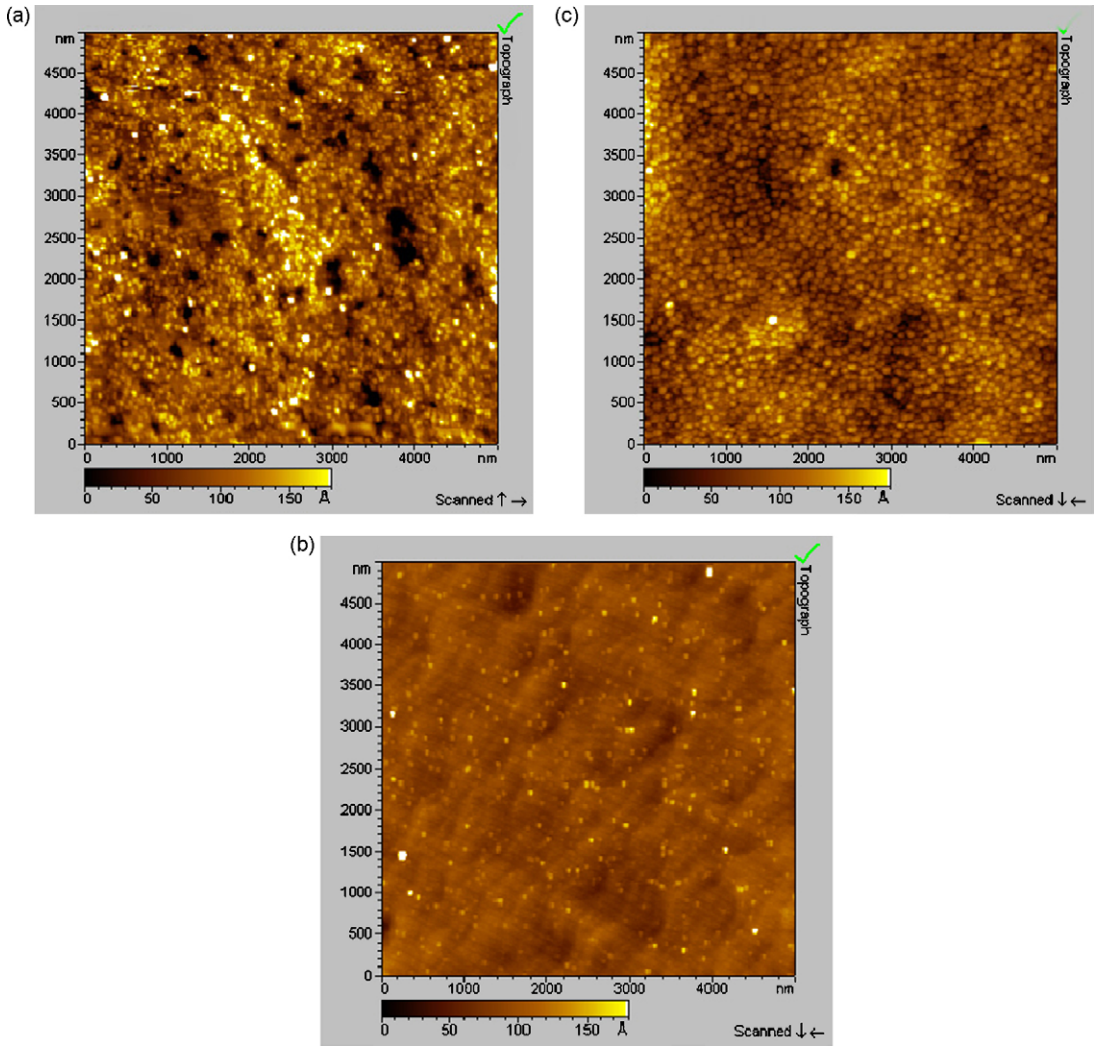

Fig. 7. 5 μm × 5 μm AFM images of $Cd_{0.74}Zn_{0.26}Se$ (a), $Cd_{0.5}Zn_{0.5}Se$ (b) and $Cd_{0.39}Zn_{0.61}Se$ (c). All compounds were obtained with 60 deposition cycles.

for deposition on the basis of the stripping charges, we also recorded the current during the whole deposition of a given compound to examine the current behavior. Different levels of current allow for the distinction of the successive steps of the compound growth, i.e. (i) bulk Se deposition, (ii) reduction of the excess of bulk Se(0) leaving the Se_{UPD} layer, (iii) formation of the UPD layer of either Cd or Zn. Fig. 6a reports the current flowing during deposition with respect to the time of deposition, in the case of a ZnSe/CdSe sequence equal to 5. Spikes in the cathodic currents are connected with the solution exchanges. It must be noted that the cathodic current involved in bulk Se deposition masks the currents involved in the UPD layers, which are only observed when the curve is enlarged (see the zoomed part of Fig. 6a). However, in our opinion, the current profile is worthwhile to be reported because of its peculiarity. Then, the highlighted profile is that of the bulk Se deposition (also reported as curve a in Fig. 6b). The sharp decrease every 5 cycles identifies bulk Se deposition on Cd. This behavior reflects the different current profiles obtained during CdSe (curve b in Fig. 6b) and ZnSe deposition (curve c Fig. 6b). Future investigation could be directed to determine the influence of parameters such as capacitance and resistivity of the growing film as well as of the presence of a different electrocatalytic effect exerted by the Cd or Zn deposited layers.

3.6. Morphological characterization

Ex situ AFM measurements were performed both on the binary and on the ternary selenides.

Fig. 7 shows 5 μm × 5 μm AFM images of $Cd_xZn_{1-x}Se$ obtained with the same 60 deposition cycles and with x values ranging between 0.3 and 0.8. The figure shows a well-defined trend of the roughness and of the cluster's size: qualitatively, both show a minimum for $x = 0.5$. The minimum is confirmed by the trend of the crystallite sizes as estimated on statistical basis. A similar trend is reported in Ref. [28], where the crystal sizes determined from XRD and SEM micrographs for chemically synthesized $Cd_xZn_{1-x}Se$ were found to decrease with increasing the Zn percentage (up to $x = 0.5$).

For $x = 0.5$ is also observed the minimum value of the root mean square (RMS) roughness parameter calculated via the

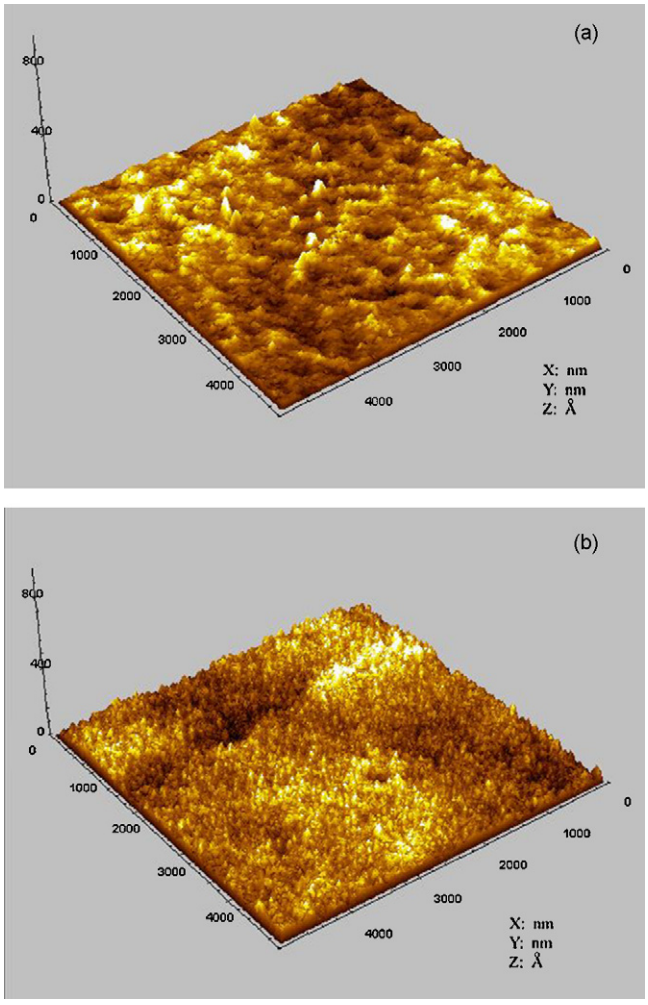

Fig. 8. Three-dimensional 5 μm × 5 μm AFM images of ZnSe (a) and $Cd_{0.39}Zn_{0.61}Se$ (b).

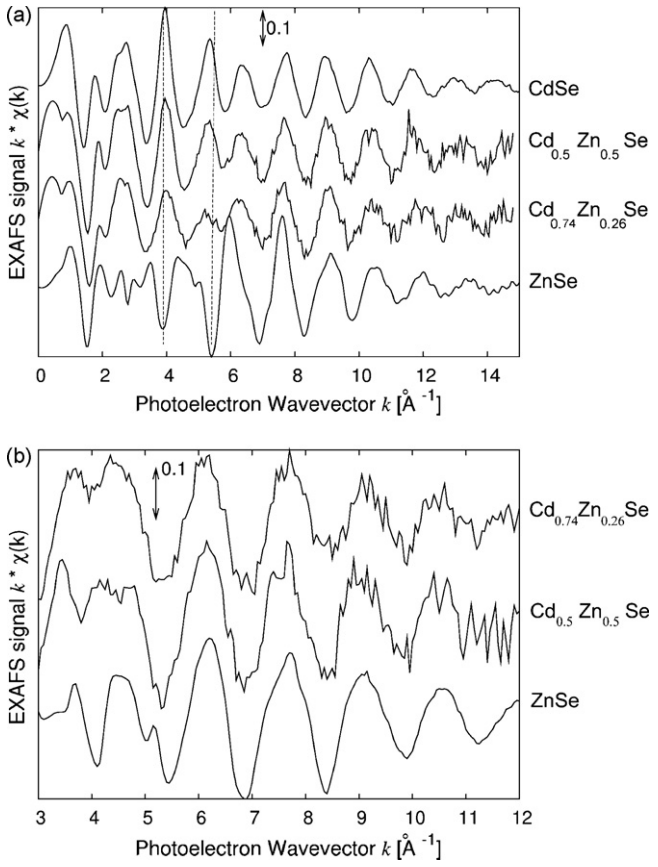

Fig. 9. EXAFS spectra at the Se–K edge (a) and Zn–K edge (b) of the samples indicated in the figures together with the model reference compounds CdSe and ZnSe. For clarity reasons, the curves relative to different samples are vertically shifted. Se is present in both reference compounds, however the EXAFS signal is extremely sensitive to its surrounding as observable in the top and bottom curves in (a). There the dashed line show an inversion of the phases between the reference compound curves.

standard formula [31,32]:

$$R_q = \sqrt{\frac{\sum_{k=1}^{M-1}\sum_{l=1}^{N-1}(Z_{k,l} - \bar{Z})^2}{MN}} \quad \text{with}$$

$$\bar{Z} = \frac{1}{MN}\sum_{k=0}^{M-1}\sum_{l=0}^{N-1} Z_{k,l} \tag{1}$$

Here $Z_{k,l}$ is the height of pixel kl; $\bar{Z}$ is the mean value of distribution; and M × N is the number of pixels and, therefore, of data points.

The calculated RMS values are included between 1 and 3 nm and, therefore, seem to be too low to represent a significant parameter. The comparison with the already investigated ternary sulfides [11] suggests that the low values are ascribable to the very thin layer obtained with 60 deposition cycles, whereas the roughness is expected to increase with the number of deposition cycles up to a limiting value. The specific investigation on increasing the film thickness was not carried out since we did not consider it crucial for the present morphological analysis.

As expected, the binary selenides appear more homogeneous. Fig. 8 shows the comparison between ZnSe and $Cd_{0.39}Zn_{0.61}Se$. However, the roughness value of ZnSe, 2.2 nm, is not far from that, 2.6 nm, of the ternary compound. This confirms our former observation that a very low roughness value is not always connected to a very smooth surface, but can also be ascribed to the high packing effect exerted by very small cluster's size [12,13].

3.7. EXAFS characterization

The experimental EXAFS spectra, extracted using the ATHENA package [33], are shown in Fig. 9, and the related Fourier transforms are shown in Fig. 10. The EXAFS spectra of the reference compounds were collected in transmission geometry using CdSe, ZnSe and ZnO powders.

A qualitative analysis of the spectra permits to immediately draw some conclusions on the first neighbors of the absorbing atoms. By observing the EXAFS spectra of the ternary compounds at 3.9 and 5.5 $Å^{-1}$, where the reference compound signals show a complete out of phase oscillation, we can notice a reduction of the oscillation with respect to the reference CdSe spectra. This already give the feeling that some disorder must be present and that an atomically mixed first coordination shell of the Se atoms is present. Moreover, no signal from the higher

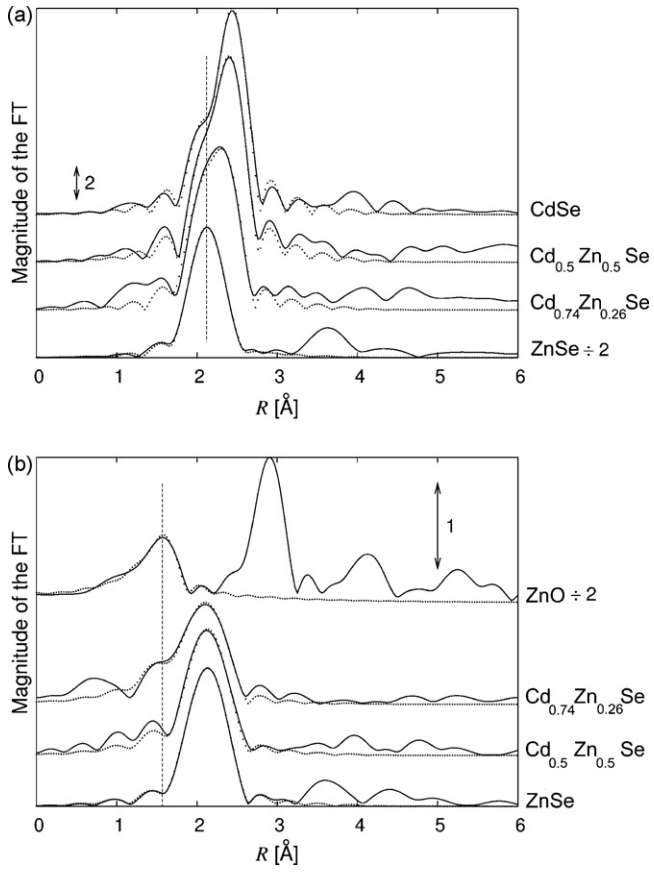

Fig. 10. Experimental (lines) and best fit (dots) moduli of the Fourier transforms of the EXAFS spectra collected at the Se–K edge (a) and Zn–K edge (b) presented in Fig. 1. The transforms were carried out in the interval $k = 3$, 13 Å^{-1} using a Hanning window and a k^3 weight (Se–K edge) or a k^2 weight (Zn–K edge). The dashed line in the Se–K edge spectra marks the position of the bond corresponding to the Se–Zn pair whereas in the Zn–K edge spectra the line marks the position of the Zn–O bond. For clarity of presentation the curves relative to different samples are shifted vertically.

coordination shells is visible in the Fourier transforms suggesting a considerable structural disorder in the particles. For what concerns the Zn–K edge the main peak in the FT of both samples coincide with that due to Zn–Se bonds in the ZnSe compound (see Fig. 10). A shoulder at low R values is also observed in the FT of sample $Cd_{0.74}Zn_{0.26}Se$ that coincides in position to that of the Zn–O bond in the crystalline ZnO. From a qualitative point of view Zn is a mixed phase of selenide plus oxide, the latter probably due to air/moisture exposure.

Data were quantitatively analyzed by generating the theoretical EXAFS signals with the Feff 8.10 code [34] starting from clusters of ZnSe [35], CdSe [36], mixed $Cd_{0.5}$ $Zn_{0.5}Se$ and ZnO [37]. The fit to the experimental data was carried out using the ARTEMIS code [38]. In the case of the data of the Se–K edge the first shell was modeled with a mixed Se–Cd and Se–Zn contribution whereas for the data at the Zn–K edge the Zn–Se and Zn–O contributions were taken into account. For each contribution the amplitude factor S_0^2 and the energy shift ΔE_0 were determined on the related model compound and kept fixed during the structural refinement of the samples. Free parameters of the fit at the

Table 1
Results of the quantitative data analysis of the Se–K edge EXAFS spectra

Parameter	CdSe	$Cd_{0.5}Zn_{0.5}Se$	$Cd_{0.74}Zn_{0.26}Se$	ZnSe
R_{ZnSe} (Å)		2.445 (7)	2.47 (1)	2.447 (1)
σ^2_{ZnSe} (Å^2)		0.0078 (3)	0.0075 (1)	0.0057 (1)
R_{CdSe} (Å)	2.621 (1)	2.612 (6)	2.610 (4)	
σ^2_{CdSe} (Å^2)	0.0047 (2)	0.0070 (3)	0.0066 (1)	
$X_{Zn} \pm dX$		0.45 (4)	0.24 (4)	

The local structural parameters like Se–Zn and Se–Cd bond length and Debye-Waller factors (DWF) are shown together with the Zn alloy content X_{Zn}. This last parameter is calculated from the number of Zn neighbors surrounding the Se, N_{Zn}.

Se–K edge were the Se–Cd and Se–Zn shell radii $R_{Se–(Zn\ or\ Cd)}$, the related Debye-Waller factors (DWF) $\sigma^2_{Se–(Zn\ or\ Cd)}$ and the number of Zn and Cd atoms surrounding Se with the constraint that their sum is equal to 4. Similar criteria were used for the Zn–K edge with the difference that here no Zn–Cd bonds are present. The results of the quantitative data analysis are reported in Table 1 for the Se–K edge and in Table 2 for the Zn–K edge.

The quantitative analysis of the EXAFS data highlights the formation of a random solid solution of the type $Cd_xZn_{(1-x)}Se$. From the atomic composition of the first shell the overall alloy composition has been derived and, in both cases, it results to be poorer in Zn with respect to the nominal value of a factor about 2. Evidence for an oxidized phase for Zn (about $5 \pm 2\%$) is found from the analysis of the Zn–K edge. The bond lengths Cd–Se and Zn–Se keep well distinct values and exhibit no appreciable trend with the composition. This means that this alloy is not described by the virtual crystal approximation (VCA), i.e. with all the atoms placed at the ideal lattice points of a zinc-blende structure (and cation locations randomly occupied by a Cd or Zn atom) and the lattice parameter linearly scaling with the composition [39]. The cation–anion bond length instead, exhibits a scarce dependence on the composition as already evi-

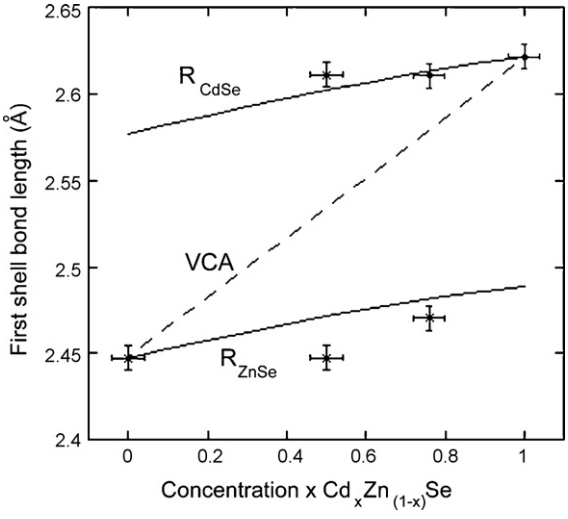

Fig. 11. Experimental values of the R_{SeCd} and R_{SeZn} bond lengths as a function of the alloy composition as determined from the number of first shell neighbors (Table 1). The results of the VFF theory [44] (solid lines) are compared with the prediction of the VCA model (dashed line) for the first shell bond length.

Table 2
Results of the quantitative data analysis of the Zn–K edge EXAFS spectra

Parameter	ZnSe	$Cd_{0.5}Zn_{0.5}Se$	$Cd_{0.74}Zn_{0.26}$ Se	ZnO
R_{ZnSe} (Å)	2.450 (3)	2.45 (1)	2.46 (2)	
σ^2_{ZnSe} (Å^2)	0.0064 (3)	0.008 (1)	0.007 (1)	
R_{ZnO} (Å)		1.96 (3)	–	1 O @1.85 (2) 3 O @1.97 (1)
σ^2_{ZnO} (Å^2)		0.002 (1)	–	0.0015 (5)
$X_{Zn} \pm dX$		0.95 (2)	1.00 (2)	

The local structural parameters like Zn–Se and Zn–O bond length and DWF are shown together with the fraction X of Zn atoms present in the alloy phase as calculated from the number of Se neighbors, N_{Se}.

denced in a number of semiconductor alloys [39–42]. In order to confirm this idea a theoretical calculation on the first shell bond length values has been carried out. This calculation was based on the valence force field (VFF) method [43] (i.e. considering an harmonic interaction potential between first neighbors) and using the procedures described in Refs. [41,44] taking into account the elastic and structural data of the CdSe and ZnSe compounds. The results are shown in Fig. 11 where it is evident that the anion–cation bond length has a faint dependence on the composition when compared to the VCA prediction.

4. Conclusions

$Cd_xZn_{1-x}Se$ were grown on Ag (1 1 1) by the ECALE method with a stoichiometry controlled by the ZnSe/CdSe deposition sequence.

The charge involved in stripping either the metal or the chalcogen atoms from $Cd_xZn_{1-x}Se$ increases linearly with the number of deposition cycles, thus supporting a layer-by-layer growth, at least concerning the first stages of the film formation. Moreover, regardless of the stoichiometry of the ternary compound obtained, the two charges are equal, thus confirming the right 1:1 stoichiometric ratio also estimated from EXAFS data.

The total amount of cations (or of Se) deposited in each deposition cycle depends on the chosen deposition sequence, i.e. on the stoichiometry, with a precise trend. More particularly, a limiting factor occurs in the x range between 0.3 and 0.7 and is maximum for $x = 0.5$. The coincidence of this range with the range of coexistence of the different structures exhibited by the $Cd_xZn_{(1-x)}Se$ thin films suggests that the reduced extent of deposition could be ascribed to the presence of structural disorder. This hypothesis is supported both by morphological and structural data: AFM images show that the cluster sizes are minimum in correspondence of $x = 0.5$, and EXAFS measurements indicate strong differences in the Zn–Se and Cd–Se bond length values.

The quantitative analysis of the EXAFS data confirm the hypothesis of $Cd_xZn_{(1-x)}Se$ formation. The different values for the bond length of the Cd–Se and Zn–Se pairs indicate that the VCA is not satisfied. The theoretical calculation of the bond length values based on the VFF method confirm the observed experimental data.

Acknowledgments

The authors are grateful to Ferdinando Capolupo and Silvano Bellandi for the preparation of the silver single crystal electrodes. F. d'Anca and F. La Manna are acknowledged for their technical support on the GILDA beamline. GILDA is a project jointly supported by CNR, INFM and INFN. The financial support of the Mur, of Fondazione del Monte dei Paschi di Siena and of the Consorzio Interuniversitario per la Scienza e Tecnologia (INSTM) is gratefully acknowledged.

References

[1] G. Hodes, I. Rubinstein, in: G. Hodes (Ed.), Electrochemistry of Nanomaterials, Wiley–VHC, 2001.
[2] B.W. Gregory, J.L. Stickney, J. Electroanal. Chem. 300 (1991) 543.
[3] C. Ma, D. Moore, Y. Ding, J. Li, Z.L. Wang, Int. J. Nanotechnol. 4 (2004) 431.
[4] L.E. Brus, J. Chem. Phys. 80 (1984) 4403.
[5] A.P. Alisivatos, A.L. Harris, N.J. Levinos, M.L. Steigerwald, L.E. Brus, J. Chem. Phys. 89 (1988) 4001.
[6] C.B. Murray, C.R. Kagan, M.G. Bawendi, Science 270 (5240) (1995) 1335.
[7] M.G. Bawendi, P.J. Carroll, W.L. Wilson, L.E. Brus, J. Chem. Phys. 96 (1992) 946.
[8] P. Reiss, J. Bleuse, A. Pron, Nano Lett. 2 (7) (2002) 781.
[9] X. Zhong, Z. Zhang, S. Liu, M. Han, W. Knoll, J. Phys. Chem. B 108 (2004) 15552.
[10] Y.M. Sung, Y.J. Lee, K.S. Park, J. Am. Chem. Soc. 128 (8) (2006) 9002.
[11] F. Loglio, M. Innocenti, G. Pezzatini, M.L. Foresti, J. Electroanal. Chem. 562 (2004) 117.
[12] M. Innocenti, S. Cattarin, F. Loglio, T. Cecconi, G. Seravalli, M.L. Foresti, Electrochim. Acta 49 (2004) 1327.
[13] M.L. Foresti, S. Milani, F. Loglio, M. Innocenti, G. Pezzatini, S. Cattarin, Langmuir 21 (2005) 6900.
[14] G. Pezzatini, S. Caporali, M. Innocenti, M.L. Foresti, J. Electroanal. Chem. 475 (1999) 164.
[15] F. Loglio, M. Innocenti, F. D'Acapito, R. Felici, G. Pezzatini, E. Salvietti, M.L. Foresti, J. Electroanal. Chem. 575 (2005) 161.
[16] P.A. Lee, P.H. Citrin, P. Eisenberger, B.M. Kincaid, Rev. Mod. Phys. 53 (1981) 769.
[17] M. Innocenti, G. Pezzatini, F. Forni, M.L. Foresti, J. Electrochem. Soc. 148 (5) (2001) C357.
[18] A. Hamelin, in: B.E. Conway, R.E. White, J.O'M. Bockris (Eds.), Modern Aspects of Electrochemistry, vol. 16, Plenum Press, New York, 1985, p. 1.
[19] A. Hamelin, L. Stoicoviciu, L. Doubova, S. Trasatti, J. Electroanal. Chem. 244 (1988) 133.
[20] T. Kurasawa, Patent Japan, 35-5619, May 23, 1960.
[21] M.L. Foresti, F. Capolupo, M. Innocenti, F. Loglio, Cryst. Growth Des. 2 (2002) 73.

[22] F. d'Acapito, S. Colonna, S. Pascarelli, G. Antonioli, A. Balerna, A. Bazzini, F. Boscherini, F.C.G. Chini, G. Dalba, I. Davoli, P. Fornasini, R. Graziola, G. Licheri, C. Meneghini, F. Rocca, L. Sangiorgio, V. Sciarra, V. Tullio, S. Mobilio, ESRF Newslett. 30 (1998) 42.
[23] S. Pascarelli, F. Boscherini, F. D'Acapito, J. Hrdy, C. Meneghini, S. Mobilio, J. Synchrotron Radiat. 3 (Pt 4) (1996) 147.
[24] G. Pezzatini, F. Loglio, M. Innocenti, M.L. Foresti, Collect. Czeck. Chem. Commun. 68 (9) (2003) 1579.
[25] C. Wei, N. Myung, K. Rajeshwar, J. Electroanal. Chem. 375 (1994) 109.
[26] M. Tomkiewicz, I. Ling, W.S. Parsons, J. Electrochem. Soc. 129 (1982) 2016.
[27] A.M. Espinosa, M.L. Toscon, M.D. Vazquez, P.S. Batanero, Electrochim. Acta 37 (1992) 1165.
[28] D. Liu, Y. Zhang, S. Zhou, J. Xiamen Univ. 28 (1989) 495.
[29] D.S. Sutrave, G.S. Shahane, V.B. Patil, L.P. Deshmukh, Turk. J. Phys. 24 (2000) 63.
[30] U. Hotje, C. Rose, M. Binnewies, Solid State Sci. 5 (2003) 1259.
[31] Reference guide of the Scanning Probe Image Processor (SPIP).
[32] J.D. Kiely, D.A. Bonnell, J. Vac. Sci. Technol. B 15 (4) (1997) 1483.
[33] M. Newville, J. Synchrotron Radiat. 8 (2001) 322.
[34] J.J. Rehr, R.C. Albers, Rev. Mod. Phys. 72 (2000) 621.
[35] R.M. Martin, Phys. Rev. B 1 (1970) 4005.
[36] E. Rabani, J. Chem. Phys. 116 (2002) 258.
[37] R.N.G. Wychoff, Crystal Structures, Interscience, New York, 1965.
[38] B. Ravel, M. Newville, J. Synchrotron Radiat. 12 (2005) 537.
[39] J.C. Mikkelsen, J.B. Boyce, Phys. Rev. Lett. 49 (1982) 1412.
[40] J. Mikkelsen, J.B. Boyce, Phys. Rev. B 28 (1983) 7130.
[41] A. Balzarotti, N. Motta, A. Kisiel, M. Zimnal-Starnawska, M. Czyzyk, M. Podgorny, Phys. Rev. B 31 (1985) 7526.
[42] J.C. Woicik, J. Pellegrino, B. Steiner, K. Miyano, S.G. Bompadre, L.B. Sorensen, T.L. Lee, S. Kalid, Phys. Rev. Lett. 79 (1997) 5026.
[43] P. Keating, Phys. Rev. 145 (1966) 637.
[44] F. D'Acapito, J. Appl. Phys. 96 (2004) 369.